THE JOURNAL OF BIOLOGICAL CHEMISTRY Vol. 278, No. 15, Issue of April 11, pp. 13257–13264, 2003
Printed in U.S.A.

Structural Basis for Dimerization of the Grb10 Src Homology 2 Domain

IMPLICATIONS FOR LIGAND SPECIFICITY*

Received for publication, November 25, 2002, and in revised form, January 19, 2003
Published, JBC Papers in Press, January 27, 2003, DOI 10.1074/jbc.M212026200

Evan G. Stein‡, Rodolfo Ghirlando§, and Stevan R. Hubbard‡¶

From the ‡Skirball Institute of Biomolecular Medicine and Department of Pharmacology, New York University School of Medicine, New York, New York 10016 and the §Laboratory of Molecular Biology, NIDDK, National Institutes of Health, Bethesda, Maryland 20892

Grb7, Grb10, and Grb14 are members of a distinct family of adapter proteins that interact with various receptor tyrosine kinases upon receptor activation. Proteins in this family contain several modular signaling domains including a pleckstrin homology (PH) domain, a BPS (between PH and SH2) domain, and a C-terminal Src homology 2 (SH2) domain. Although SH2 domains are typically monomeric, we show that the Grb10 SH2 domain and also full-length Grb10γ are dimeric in solution under physiologic conditions. The crystal structure of the Grb10 SH2 domain at 1.65-Å resolution reveals a non-covalent dimer whose interface comprises residues within and flanking the C-terminal α helix, which are conserved in the Grb7/Grb10/Grb14 family but not in other SH2 domains. Val-522 in the BG loop (BG3) and Asp-500 in the EF loop (EF1) are positioned to interfere with the binding of the P+3 residue of a phosphopeptide ligand. These structural features of the Grb10 SH2 domain will favor binding of dimeric, turn-containing phosphotyrosine sequences, such as the phosphorylated activation loops in the two β subunits of the insulin and insulin-like growth factor-1 receptors. Moreover, the structure suggests the mechanism by which the Grb7 SH2 domain binds selectively to pTyr-1139 (pYVNQ) in Her2, which along with Grb7 is co-amplified in human breast cancers.

Grb10 is a member of a family of adapter proteins including Grb7 and Grb14, which have been identified as putative downstream effectors of receptor tyrosine kinases (1). Proteins in this family contain several modular domains including an N-terminal proline-rich region, a Ras-associated-like domain, a pleckstrin homology (PH)[1] domain, a short region known as the BPS (between PH and SH2) or PIR (phosphorylated insulin receptor-interacting region) domain, and a C-terminal Src homology 2 (SH2) domain. Grb10 has multiple alternatively spliced forms (α–ζ), which differ in their N-terminal region including the PH domain.

The BPS/PIR and SH2 domains of Grb7/Grb10/Grb14 have been implicated in the interaction with activated receptor tyrosine kinases. The BPS domain is a structurally uncharacterized region of ~50 residues that is unique to this family of adapter proteins. The SH2 domain, found in many signaling proteins, is a well characterized protein module of ~100 residues that binds phosphotyrosine-containing sequences (2, 3). The BPS domains of Grb7/Grb10/Grb14 bind to the phosphorylated insulin and insulin-like growth factor-1 (IGF1) receptors (4–6). The SH2 domains of Grb7/Grb10/Grb14 also interact with the insulin and IGF1 receptors (4, 5, 7–11) and, in addition, have been shown to mediate the interaction with the epidermal growth factor receptor (4, 12), Her2 (epidermal growth factor receptor family) (13, 14), platelet-derived growth factor receptor-β (10, 15, 16), Ret (17), EphB1 (18), Kit (19), Tie2 (20), and fibroblast growth factor receptor-1 (21).

The roles of Grb10 family members in growth factor-mediated signaling have not been clearly established. Most studies have investigated the effects of these adapter proteins on mitogenesis. Several studies have indicated that Grb10 and Grb14 negatively regulate insulin- and IGF1-mediated mitogenic signaling (5, 7, 8, 22), possibly through direct inhibition of receptor catalytic activity by the BPS domain (23, 24). In contrast, Grb10 has been reported to enhance platelet-derived growth factor-stimulated mitogenesis (16). Moreover, in many human breast cancer cell lines, Grb7 is co-overexpressed with and bound to Her2 and thus might potentiate Her2 signaling (13).

To begin to understand the structural basis for the interaction of Grb10 with the insulin and IGF1 receptors, we have determined the crystal structure of the SH2 domain of Grb10. Although SH2 domains typically function as monomers, gel filtration and sedimentation equilibrium studies show that the Grb10 SH2 domain and full-length Grb10γ are dimeric in solution. The crystal structure reveals the molecular basis for dimerization of the Grb10 SH2 domain. The dimer interface comprises residues in the C-terminal half of the domain, which are conserved in the Grb7/Grb10/Grb14 family. Several sequence and structural features of the Grb10 SH2 domain including its mode of dimerization are predicted to discriminate against binding of canonical, extended phosphotyrosine-containing sequences and favor binding of turn-containing sequences.

* This work was supported by National Institutes of Health Grant DK52916 (to S. R. H.). Financial support for beamline X12C of the National Synchrotron Light Source comes principally from the National Institutes of Health and the Department of Energy. The costs of publication of this article were defrayed in part by the payment of page charges. This article must therefore be hereby marked "*advertisement*" in accordance with 18 U.S.C. Section 1734 solely to indicate this fact.

The atomic coordinates and structure factors (code 1NRV) have been deposited in the Protein Data Bank, Research Collaboratory for Structural Bioinformatics, Rutgers University, New Brunswick, NJ (http://www.rcsb.org/).

¶ To whom correspondence should be addressed: Skirball Institute of Biomolecular Medicine, New York University School of Medicine, 540 First Ave., New York, NY 10016. Tel.: 212-263-8938; Fax: 212-263-8951; E-mail: hubbard@saturn.med.nyu.edu.

[1] The abbreviations used are: PH, pleckstrin homology; SH2, Src homology 2; BPS, between PH and SH2; IGF, insulin-like growth factor; P+3, third residue after phosphotyrosine; WT, wild type; IRK, insulin receptor kinase domain; LCK, lymphocyte kinase.

EXPERIMENTAL PROCEDURES

Production of Grb10 Proteins—Both wild-type and mutant (Phe-515 → Arg) full-length human Grb10γ (residues 1–536) and BPS-SH2 constructs (residues 357–536) were subcloned into expression vector pET21 (Novagen). All of the constructs were verified by DNA sequencing. *Escherichia coli* strain BL21(DE3) was transformed with the plasmids, and cultures were grown in Luria Broth at 37 °C to an A_{600} of 0.8. Protein expression was induced by the addition of isopropyl-1-thio-β-D-galactopyranoside (1.0 mM final) for 3 h at 30 °C. Bacteria were harvested by centrifugation, resuspended in lysis buffer (20 mM Hepes, pH 7.5, 0.1% Triton X-100, 1 mM PMSF, and Complete protease inhibitor tablets (Roche Molecular Biochemicals)), and lysed by French press. The lysate was centrifuged at 20,000 × *g* for 1 h, and the supernatant was collected. Proteins were purified from the soluble fraction using cation-exchange chromatography (Fractogel, EM Science) followed by gel filtration chromatography (Superdex-75, Amersham Biosciences).

The isolated Grb10 SH2 domains, wild type ($SH2^{WT}$), and Phe-515→Arg mutant ($SH2^{F515R}$) were obtained by mixing purified BPS-SH2 (4 mg/ml final) at room temperature with elastase (10 μg/ml final) for 2.5 h. The resulting proteolyzed fragments were purified by gel filtration chromatography (Superose-12, Amersham Biosciences). A 12,340-Da fragment was verified to be the SH2 domain (residues 429–533) by mass spectrometry and N-terminal sequencing. Protein concentrations were determined using calculated extinction coefficients (25).

Crystallization and X-ray Analysis—Crystals of the Grb10 SH2 domain were grown by vapor diffusion at 4 °C using the hanging drop method. 2 μl of protein solution (4 mg/ml in 20 mM HEPES, pH 7.5, and 100 mM NaCl) was mixed with 2 μl of a crystallization buffer (10% polyethylene glycol 8000, 100 mM HEPES, pH 7.5, and 5 mM Tris[2-carboxyethyl]phosphine, and the drop was suspended over 500 μl of the crystallization buffer and allowed to equilibrate for 2 days. The equilibrated drops were then suspended over a reservoir buffer that contained 15% polyethylene glycol 8000. The crystals belong to the monoclinic space group $P2_1$ with unit cell dimensions a = 28.82 Å, b = 49.04 Å, c = 79.61 Å, and β = 96.62°. There are two molecules of the SH2 domain in the asymmetric unit yielding a solvent content of ~46%. Crystals were equilibrated in a cryoprotectant of reservoir buffer plus 10% glycerol before being flash-frozen in liquid propane. Data were collected at beamline X12C at the National Synchrotron Light Source, Brookhaven National Laboratory. The data were processed using Denzo and Scalepack (26). A molecular replacement solution was found with AMoRE (27) using a homology model (28) of the Grb10 SH2 domain based on the crystal structure of the N-terminal SH2 domain of Syk (Protein Data Bank code 1A81) (29). Simulated annealing, rigid-body, positional, and B-factor refinement were carried out using CNS (30). Model building was performed with O (31). Buried surface area in the dimer interface was calculated with CNS (30) using a probe radius of 1.4 Å.

Gel Filtration Chromatography and Gel-shift Assays—Gel filtration chromatography was performed on a Superose-12 10/30 column, which was equilibrated in 20 mM HEPES, pH 7.5, 100 mM NaCl, and 1 mM dithiothreitol for all Grb10 samples and protein standards. The column flow rate was 0.4 ml/min. For the gel-shift studies, 1 μl of purified $BPS\text{-}SH2^{WT}$ or $BPS\text{-}SH2^{F515R}$ at 200 μM was mixed with 1 μl of the tris-phosphorylated insulin receptor kinase domain (IRK) (residues 978–1283) at 100 μM and prepared essentially as described by Hubbard (32). Mixtures were loaded onto a 20% native PhastGel and electrophoresed with the PhastGel system (Amersham Biosciences). The gels were stained with PhastGel Blue R.

Sedimentation Equilibrium Ultracentrifugation—Samples of the Grb10 SH2 domain were prepared in 50 mM HEPES, pH 7.5, and 100 mM NaCl and analyzed at loading concentrations of A_{280} = 0.10, 0.21, 0.28, 0.41, and 0.51. Sedimentation equilibrium experiments were conducted at 4.0 °C in a Beckman Optima XL-A analytical Ultracentrifuge. Samples (loading volume of 160 μl) were studied at different rotor speeds corresponding to 12,000, 14,000, 16,000, and 18,000 rpm. Data were acquired as an average of 8 absorbance measurements at a nominal wavelength of 280 nm and a radial spacing of 0.001 cm. Equilibrium was achieved within 48 h. Data were initially analyzed in terms of a single ideal solute to obtain the buoyant molecular mass, $M_1(1 - v_1\rho)$, using the Optima XL-A data analysis software (Beckman). The values of M_1 were calculated using densities (ρ) at 4.0 °C obtained from standard tables and a calculated v_1 = 0.7389 ml/g (33). Data from sedimentation equilibrium experiments performed at loading concentrations of A_{280} = 0.21 and 0.10 were analyzed in terms of reversible monomer-dimer equilibria, essentially as described by Jenkins *et al.* (34).

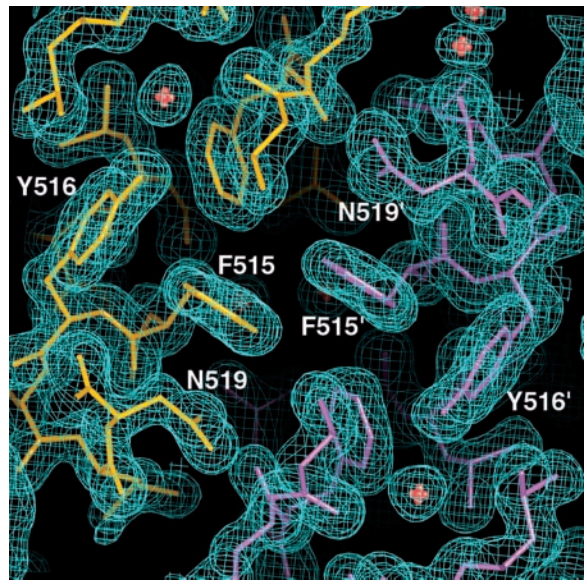

FIG. 1. **Electron density map in the Grb10 SH2 dimer interface.** The $2F_o - F_c$ electron density map (1.65-Å resolution, 1σ contour) is shown as wire mesh (*cyan*), and the two SH2 domain protomers (after refinement) are shown in a *stick representation colored* in *gold* and *purple*. Ordered water molecules are indicated with *red crosses*. Selected residues are labeled. An *apostrophe* in the label differentiates residues in the *purple* protomer from the *gold* protomer.

TABLE I
X-ray data collection and refinement statistics

Data collection	
Resolution (Å)	30–1.65
Observations	74,325
Unique reflections	26,168
Completeness[a] (%)	99.6 (99.2)
R_{sym}[a,b] (%)	4.5 (37.0)
Refinement	
Number of atoms:	
Protein	1,688
Water	185
Resolution (Å)	30–1.65
Reflections	25,051
R_{cryst}/R_{free}[c] (%)	22.3/24.0
Root mean square deviations:	
Bond lengths (Å)	0.005
Bond angles (°)	1.2
B-factors[d] (Å^2)	1.3
Average B-factors (Å^2):	
All atoms	19.7
Protein	18.7
Water	29.2

[a] The overall (30–1.65 Å) value is given first with the value in the highest resolution shell (1.69–1.65 Å) given in parenthesis.
[b] $R_{sym} = 100 \times \Sigma|I - \langle I \rangle|/\Sigma I$.
[c] $R_{cryst} = 100 \times \Sigma||F_o| - |F_c||/\Sigma|F_c|$, where F_o and F_c are the observed and calculated structure factors, respectively ($F_o > 0\sigma$). R_{free} was determined from 5% of the data.
[d] For bonded protein atoms.

RESULTS

Overall Description of the Grb10 SH2 Domain Structure—The crystal structure of the SH2 domain of Grb10γ was solved by molecular replacement using a homology model (28) based on the N-terminal SH2 domain of Syk (29) and was refined at 1.65-Å resolution. A $2F_o - F_c$ electron density map is shown in Fig. 1, and the crystallographic statistics are given in Table I. The overall structure of the Grb10 SH2 domain is similar to those of other SH2 domains (2), possessing a core anti-parallel β sheet flanked on either side by an α helix (Fig. 2*A*). The asymmetric unit comprises two SH2 domains that form a non-covalent dimer with the two protomers related by a molecular 2-fold axis. The atomic model includes residues 429–533 with

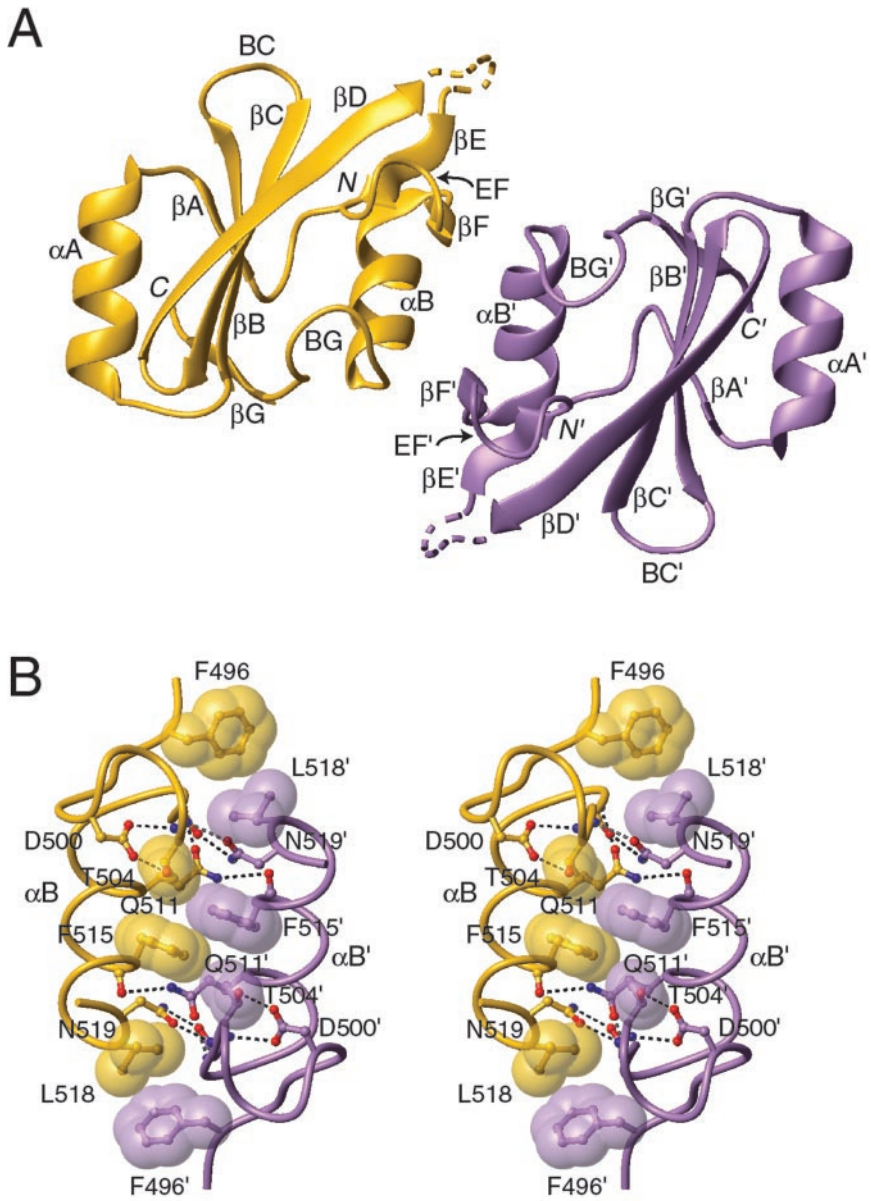

FIG. 2. **Crystal structure of the Grb10 SH2 dimer.** *A*, *ribbon diagram* of the Grb10 SH2 dimer. The two individual SH2 domain protomers are *colored gold* and *purple*. Secondary structure elements are labeled using the nomenclature described previously (35), and labeling for the two protomers is differentiated by the use of an *apostrophe* for the second (*purple*) protomer. The N and C termini are indicated by *N* and *C*. The *BC*, *EF*, and *BG* loops are explicitly labeled, and the disordered *DE* loops (residues 490–494) are depicted with *broken lines*. The noncrystallographic 2-fold axis is perpendicular to the page. *B*, stereoview of the dimer interface. The orientation and coloring of the protomers is the same as in *A*. The backbone of the protein is shown in a *coil representation*. Backbone and side chain atoms in the dimer interface are shown in *ball-and-stick representation*. Hydrogen bonds are represented by *dashed black lines*, and residues making hydrophobic contacts are shown with semi-transparent van der Waals surfaces. Carbon atoms are *colored* either *gold* or *purple*, oxygen atoms are shown in *red*, and nitrogen atoms are in *blue*.

the exception of residues 490–494 (DE loop), which are disordered in both molecules. The overall root mean square deviation in the Cα positions in the two protomers is 0.5 Å.

The dimer interface comprises residues from the C-terminal half of the SH2 domain (Fig. 2*B*), primarily in α-helix B (αB), and is a composite of hydrophobic and hydrophilic interactions. In the middle of the interface is Phe-515 (αB8; SH2 domain nomenclature is from Eck *et al.* (35)), which is packed against Phe-515 and Thr-504 (βF1) from the other protomer (designated Phe-515′ and Thr-504′). The side chain of Gln-511 (αB4) is hydrogen-bonded to the backbone of Asp-514′ as well as to the backbone of Asp-508 and the side chain of Ser-507. The side chain of Asn-519 (αB12) makes two hydrogen bonds to the backbone of Lys-505′. The interface is capped on each end through packing of Leu-518 (αB11) with Phe-496′ (βE1). The total surface area buried in the interface is 780 Å^2 (~390 Å^2/protomer, representing 6.6% of the surface area). A sequence alignment of the SH2 domains of Grb7/Grb10/Grb14 (Fig. 3) shows that the residues in the Grb10 SH2 dimer interface are strictly conserved with the exception of Phe-496, which in Grb7 is conservatively substituted with tyrosine.

Absence of a P+3 Binding Pocket and Aberrant BC Loop in the Grb10 SH2 Domain—Previous structural studies have shown that phosphotyrosine-containing peptides generally bind in an extended conformation perpendicular to the β sheet of the SH2 domain (2). In a typical SH2-phosphopeptide interaction, two deep pockets in the SH2 domain engage the phosphotyrosine (P residue) and the P+3 residue of the phosphopeptide (36), which is often hydrophobic. The binding pocket for phosphotyrosine comprises residues from αA, βB, βD, and the BC loop. An invariant arginine (βB5; Arg-462 in Grb10) salt-bridges with the phosphate moiety of the phosphotyrosine. The binding pocket for the P+3 residue is formed between the EF and BG loops.

A superposition of the Grb10 SH2 domain and the Src SH2 domain with bound phosphopeptide (36) indicates that the binding pocket for the P+3 residue in the Grb10 SH2 domain is absent (Fig. 4*A*) because of Val-522 in the BG loop (BG3) (Fig. 4*B*). This residue along with Asp-500 in the EF loop (EF1) seals off the peptide binding cleft at the P+3 position. Asp-500 is hydrogen-bonded to both the backbone and side chain of Thr-504 (Fig. 2*B*), a residue in the dimer interface, as well as to the side chain of Ser-498. Val-522 is conserved in Grb14 and is an isoleucine in Grb7. The BG loop of Grb10 is relatively short and

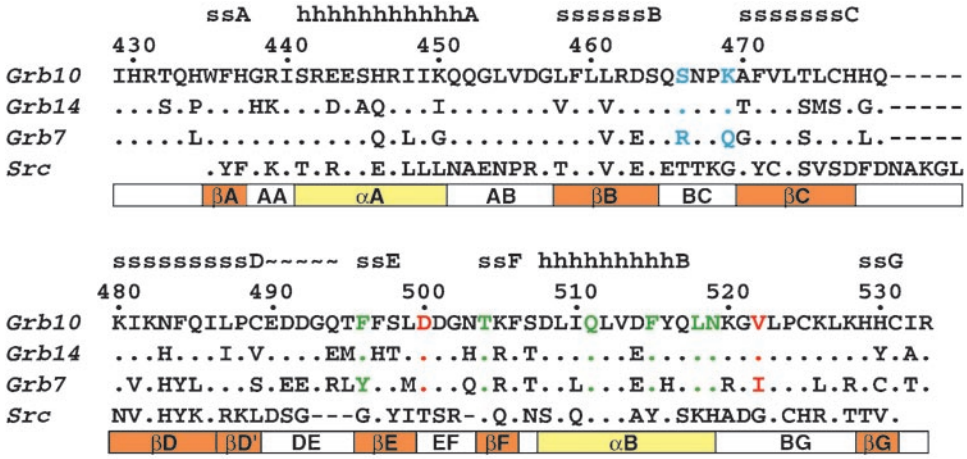

FIG. 3. **Structure-based sequence alignment of the SH2 domains of Grb7, Grb10, and Grb14.** The sequences are for the human proteins. A *dot* (·) in the alignment indicates sequence identity to Grb10. The location and length of the secondary structure elements as determined from the Grb10 crystal structure are shown above the alignment with α helices indicated by "*h*," β strands indicated by "*s*," and disordered residues indicated by "~." Residues in the dimer interface are shown in *green*. Residues in Grb10 that are poised to block binding of the P+3 residue of a phosphopeptide are shown in *red*. Residues that are predicted to affect phosphate coordination by the BC loop are shown in *blue*. The canonical SH2 domain secondary structure assignments (35) are shown below the alignment. *Orange boxes* represent β strands, and *yellow boxes* represent α helices. For example, BC2 refers to the second residue in the BC loop (counting in the *bottom boxes*), which is Ser-466 in Grb10, and αB8 refers to the eighth residue in αB, which is Phe-515 in Grb10.

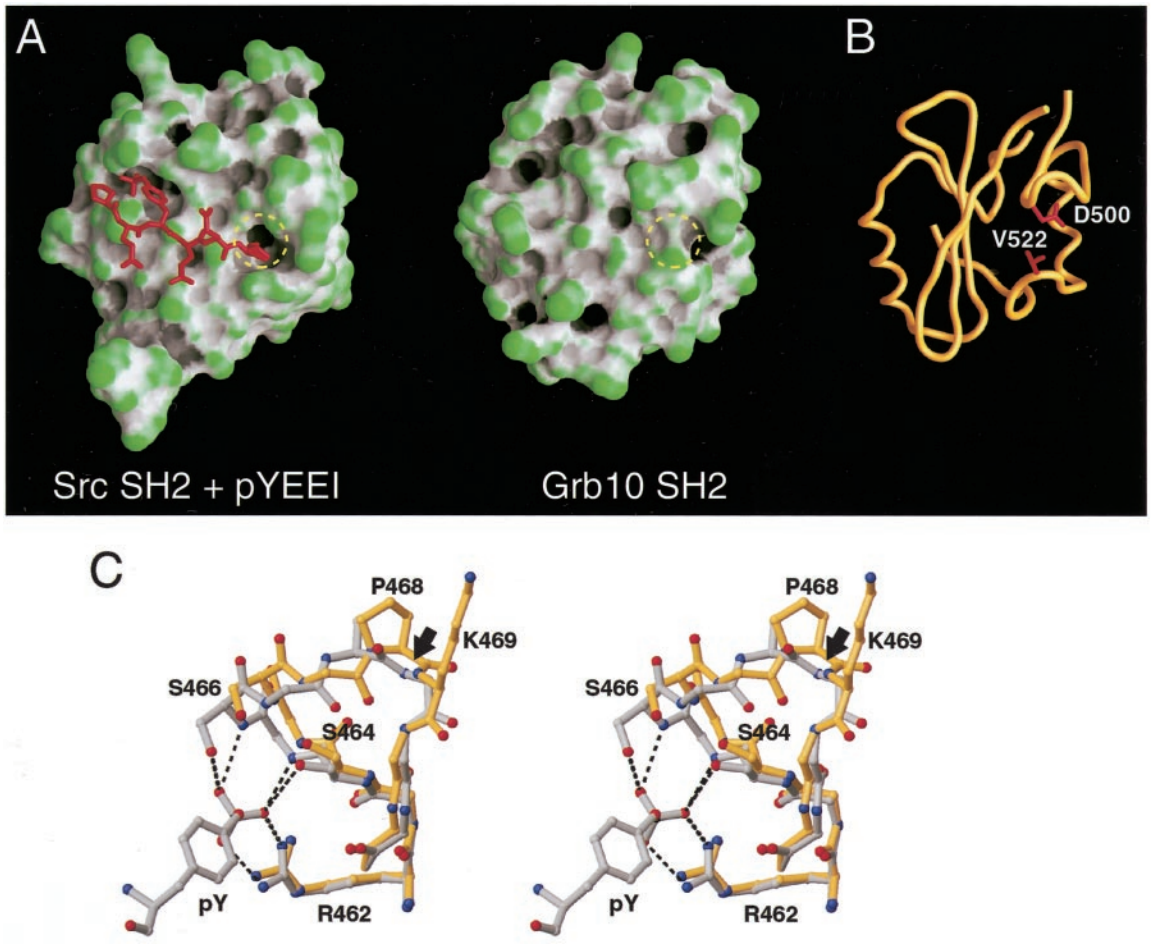

FIG. 4. **Absence of a P+3 binding pocket and aberrant BC loop in the Grb10 SH2 domain.** *A*, surface representations of the Src SH2 domain with bound pYEEI phosphopeptide (*left*) (36) and of one of the Grb10 SH2 domain protomers (*right*). The phosphopeptide is shown in a *red stick representation*. The orientations of the two SH2 domains are the same, obtained through Cα superposition of the core β sheet. The surface coloring is according to curvature: *green*, high convex curvature; *black*, high concave curvature. The binding pocket for the P+3 residue of the phosphopeptide (isoleucine) in the Src SH2 domain is indicated by a *dashed yellow circle*. The corresponding location in the Grb10 SH2 domain is also indicated by a *dashed yellow circle*, which shows that the P+3 binding pocket is absent in the Grb10 SH2 domain. *B*, backbone representation of the Grb10 SH2 domain (same orientation/scale as in *right panel* of *A*) with residues Asp-500 (EF1) and Val-522 (BG3) responsible for the lack of a P+3 binding pocket shown in a *red stick representation*. *C*, stereoview of a superposition between the BC loops of the Grb10 SH2 domain and the LCK SH2 domain (35). Bonds and carbon atoms of Grb10 and LCK are *colored gold* and *gray*, respectively. Oxygen atoms are *colored red*, nitrogen atoms are *blue*, and phosphorus atoms are *black*. Only selected (labeled) side chains are shown. Others are truncated to Cα. The residues

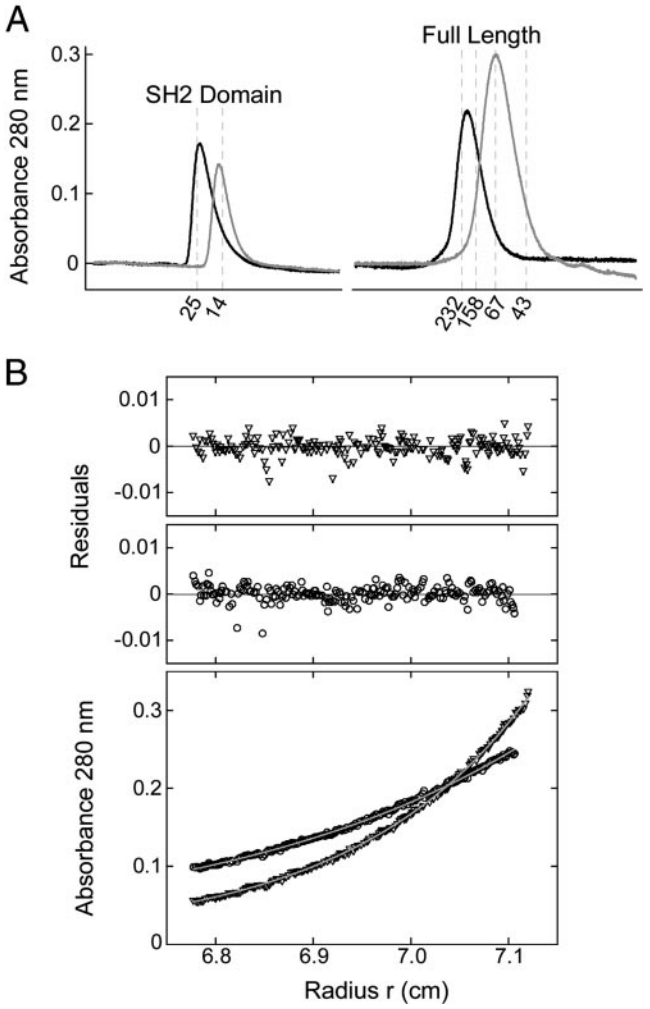

FIG. 5. **Solution studies of the Grb10 SH2 domain and full-length Grb10γ.** *A*, *left*, 100 μl of the wild-type (*black*) or mutant (Phe-515 → Arg) (*gray*) Grb10 SH2 domain were loaded onto a Superose-12 size-exclusion column at a concentration of ~250 μM for each; *right*, 100 μl of wild-type (*black*) or mutant (Phe-515 → Arg) (*gray*) full-length Grb10γ were loaded onto a Superose-12 column at 40 or 50 μM, respectively. The elution positions of standards are indicated by *dashed vertical lines* (catalase (232 kDa); aldolase (158 kDa); albumin (67 kDa); ovalbumin (43 kDa); chymotrypsinogen A (25 kDa); and ribonuclease A (14 kDa)). *B*, sedimentation equilibrium profiles at 280 nm (*bottom*) and the corresponding residuals (*top*) for the Grb10 SH2 domain at 16,000 (*triangles*) and 12,000 (*circles*) rpm and 4.0 °C. The initial loading concentration corresponds to an A_{280} of 0.21. The *lines* (*gray*) through the data represent the best fit for a reversible monomer-dimer equilibrium. The fitting yields a $\ln(K_a)$ value of 13.8 ± 0.3, corresponding to a K_d of 1.0 ± 0.4 μM. The fitting of data (data not shown) for samples at an initial loading concentration of A_{280} = 0.10 yielded a K_d of 2.8 ± 0.5 μM.

of the same length as the BG loops in Src, Abl, and Zap70. In these other SH2 domains, a glycine is present at the position of Val-522 (BG3); lack of a side chain at this position provides the pocket for the P+3 residue of the phosphopeptide.

The BC loop in SH2 domains interacts with the phosphate group of the phosphopeptide. A majority of SH2 domains possess a five-residue BC loop, and nearly all of these contain a glycine at the end of the loop (BC5) including Src, Shp2, Abl, and Grb2. The BC loop in the SH2 domains of Grb7/Grb10/Grb14 is also five residues long, but it ends with lysine (Grb10/14) or glutamine (Grb7) rather than glycine. The backbone dihedral angles (ϕ, ψ) for this glycine in the structure of the ligand-bound LCK (Src family) SH2 domain (35) are (108 and −17°), a combination that is much less energetically favorable for a residue with a side chain. In the Grb10 SH2 domain structure, the backbone dihedral angles of Lys-469, particularly ϕ, are substantially different (−114 and 6°), resulting in a difference in conformation of the BC loop (Fig. 4*C*). The non-glycl residue at BC5 in Grb7/Grb10/Grb14 is likely to impair phosphate coordination by the BC loop.

Solution Studies of the Grb10 SH2 Domain and Full-length Grb10γ—During purification, the Grb10 SH2 domain eluted from a gel filtration column at a volume corresponding to a dimer, consistent with the crystallographic results. Based on the key position of Phe-515 at the center of the dimer interface (Figs. 1 and 2*B*), mutant Grb10γ proteins (SH2 domain and full-length) were generated with the substitution Phe-515 → Arg, which would be predicted to yield a monomeric SH2 domain. The oligomeric properties of the purified wild-type and mutant proteins were examined by gel filtration chromatography and sedimentation equilibrium ultracentrifugation.

As shown in Fig. 5*A*, the wild-type Grb10 SH2 domain (molecular mass = 12.4 kDa) elutes at a volume consistent with a dimer, whereas the Phe-515 → Arg mutant elutes at a volume corresponding to a monomer. Sedimentation equilibrium experiments were performed to further analyze the oligomeric properties of the wild-type SH2 domain. At a high loading concentration (A_{280} = 0.28, ~40 μM), an analysis in terms of a single ideal solute yielded buoyant molecular masses that were independent of the rotor speed, indicating that the sample was monodisperse. The experimentally determined molecular mass of 26,310 ± 480 g/mol shows that the SH2 domain is dimeric in solution. At lower loading concentrations (A_{280} = 0.10 and 0.21), modeling of the data in terms of a single ideal solute returned buoyant masses lower than that expected for a dimer but larger than that expected for a monomer. Data for the two concentrations were analyzed globally in terms of a reversible monomer-dimer equilibrium. Excellent fits were obtained (Fig. 5*B*) yielding K_d values of 1.0 ± 0.4 μM (A_{280} 0.21) and 2.8 ± 0.5 μM (A_{280} 0.10). Therefore, the Grb10 SH2 domain undergoes reversible dimerization with a K_d of ~2 μM.

An analysis by gel filtration chromatography of full-length Grb10γ (molecular mass = 60.8 kDa) indicates that Grb10γ is also oligomeric in solution with an elution volume just greater (lower molecular mass) than that of the 232-kDa molecular mass standard (Fig. 5*A*). This elution position suggests either a compact tetramer or an elongated dimer. A trimer is unlikely because of the observed 2-fold symmetry of the SH2 domain. The full-length Grb10γ mutant (Phe-515 → Arg) elutes at the same volume as the 67-kDa standard, consistent with a monomeric protein.

Interaction of Grb10 BPS-SH2 with the Phosphorylated Insulin Receptor Kinase—Interaction of full-length Grb10 with the insulin receptor involves both the SH2 domain and the BPS domain (4). We have previously shown that the purified Grb10 BPS-SH2 protein binds to the tris-phosphorylated form of the insulin receptor kinase domain (IRK^{3P}), but not to the unphosphorylated form (23). We analyzed binding of wild-type Grb10 BPS-SH2 (dimeric) or mutant BPS-SH2 (Phe-515 → Arg; monomeric) to IRK^{3P} by native-gel electrophoresis (Fig. 6*A*). The gel-shift assay shows that both wild-type and mutant BPS-SH2 form a complex with IRK^{3P}, but the mobility (a function of size,

in LCK corresponding to the labeled residues in Grb10 are Arg-154 (Arg-462 in Grb10), Ser-156 (Ser-464), Ser-158 (Ser-466), Ala-160 (Pro-468), and Gly-161 (Lys-469). The *black arrow* points to the major difference in backbone conformation in the BC loop between Pro-468/Lys-469 in Grb10 and Ala-160/Gly-161 in LCK. Hydrogen bonds to the phosphotyrosine moiety in the LCK structure are shown as *black dashed lines*.

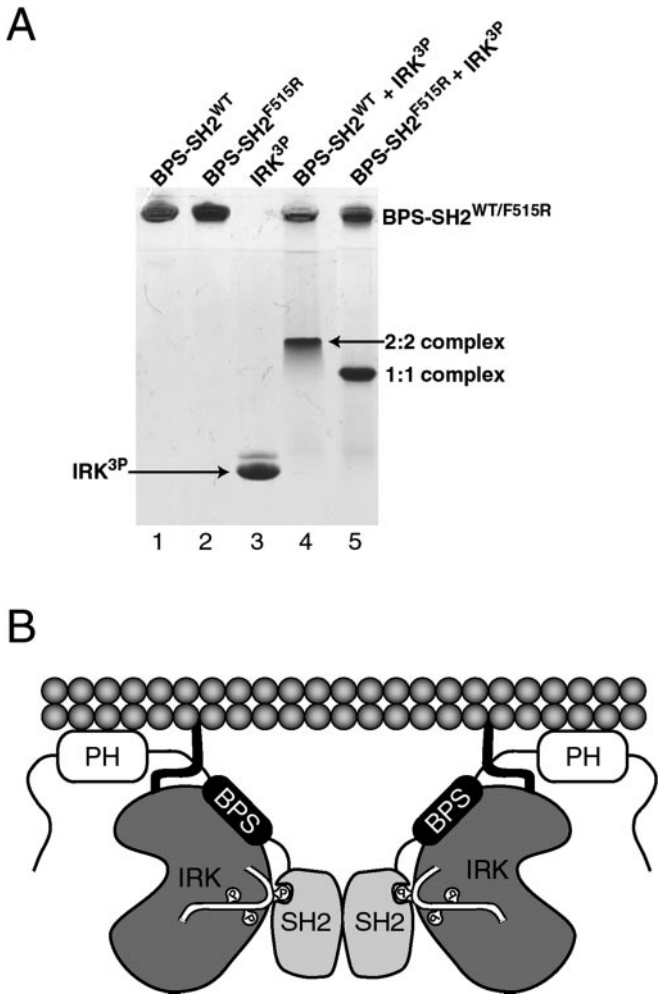

FIG. 6. **Interaction between Grb10 BPS-SH2 and tris-phosphorylated IRK.** *A*, native gel analysis of complex formation between tris-phosphorylated IRK (*IRK^{3P}*) and either wild-type dimeric BPS-SH2 (*BPS-SH2^{WT}*) or mutant (Phe-515 → Arg) monomeric BPS-SH2 (*BPS-SH2^{F515R}*). The individual BPS-SH2 proteins (wild type and mutant, *lanes 1* and *2*) do not migrate into the gel because of their high pI, whereas IRK^{3P} alone migrates with high mobility (*lane 3*). The protein complex produced by mixing BPS-SH2^{WT} with IRK^{3P} (*lane 4*) has a slower mobility than the complex between BPS-SH2^{F515R} and IRK^{3P} (*lane 5*), suggesting a 2:2 stoichiometry for BPS-SH2^{WT} + IRK^{3P} and a 1:1 stoichiometry for BPS-SH2^{F515R} + IRK^{3P}. *B*, model for the interaction of Grb10γ with the insulin receptor. The Grb10γ SH2 dimer binds to the activation loops of the two tyrosine kinase domains of the insulin receptor β subunits, facilitated by binding of the PH domain to phosphatidylinositol phosphates in the plasma membrane (spheres). The BPS domain of Grb10γ binds to an unidentified site on the kinase domain. The extracellular portion of the insulin receptor is not shown, nor is the Grb10γ Ras-associated-like domain, which is N-terminal to the PH domain.

charge, and shape) of the mutant complex is significantly greater than the mobility of the wild-type complex. A change in oligomeric state notwithstanding, the addition of one positive charge (Phe-515 → Arg) to the protein complex would reduce mobility in the native gel. These gel-shift results are consistent with formation of a 2:2 complex between wild-type BPS-SH2 and IRK^{3P} and a 1:1 complex between mutant BPS-SH2 and IRK^{3P}.

DISCUSSION

The crystal structure of the Grb10 SH2 domain reveals a 2-fold symmetric dimer with residues in and flanking the C-terminal α helix (αB) mediating the interaction between the two protomers (Fig. 2). All of the residues in the dimer interface are conserved in the Grb7/Grb10/Grb14 family with the exception of the conservative substitution of Phe-496 → Tyr in Grb7 (Fig. 3). Inspection of a sequence alignment of SH2 domains indicates that only members of this adapter family contain hydrophobic residues at positions βE1 (Phe-496), αB8 (Phe-515), and αB11 (Leu-518), suggesting that the observed mode of dimerization of the Grb10 SH2 domain is unique to this family.

SH2 domains are typically monomeric, both in solution and in crystal structures. Two crystal structures of dimeric SH2 domains have been reported previously. In a crystal structure of the SH2 domain of Shc (37), a disulfide-bonded dimer was observed, which would not be favored in the reducing environment of the cytosol. Moreover, the Shc SH2 domain is monomeric in solution at physiologic pH (37). A domain-swapped dimeric form of the Grb2 (unrelated to Grb7/Grb10/Grb14) SH2 domain has been observed crystallographically (38), as has a monomeric form (39), but this dimer is likely to be an artifact of expression as a glutathione *S*-transferase fusion protein (40).

From gel filtration and sedimentation equilibrium experiments (Fig. 5), the Grb10 SH2 domain is dimeric in solution at physiologic pH with a K_d of ~2 μM. Substitution of Phe-515 in the dimer interface with arginine (or alanine, data not shown) yields a monomeric SH2 domain. This provides strong evidence that the crystallographic dimer is also the solution dimer. Whether full-length Grb10γ is an elongated dimer or a compact tetramer is not established unequivocally from the gel filtration experiments. The observation that the point mutation Phe-515 → Arg yields a monomeric protein rather than an intermediate dimeric protein suggests that Grb10γ is an elongated dimer. This supposition is plausible given the multidomain composition of Grb7/Grb10/Grb14 (Ras-associated-like, PH, BPS, and SH2). The gel filtration data indicate that oligomerization is mediated wholly or in large part by SH2 dimerization, although our data do not rule out the possibility that other regions in Grb10γ make minor contributions to oligomerization. A modest K_d of ~2 μM for SH2 domain dimerization implies that, depending on cellular levels of Grb10γ, the protein could be monomeric in the cytosol. The PH domain of Grb10γ is likely to interact with phosphatidylinositol phosphates as has been demonstrated for the Grb7 PH domain (41). Localization of Grb10γ to the plasma membrane via the PH domain will increase the effective protein concentration, promoting SH2 domain-mediated dimerization of Grb10γ.

A previous study (42) on the oligomerization state of Grb10 has been reported in which it was concluded that Grb10β/ζ is a tetramer. In that study, a CHO cell lysate containing transfected Grb10β (called Grb10α in Ref. 42) or Grb10ζ (called Grb10γ) was run on a gel filtration column and Grb10β/ζ was detected by Western blot analysis. Our gel filtration and sedimentation equilibrium experiments were performed with highly purified Grb10γ at relatively high concentrations, which would favor higher order oligomerization, from which we conclude that Grb10γ is most likely to be a dimer. Also in the study by Dong *et al.* (42), yeast two-hybrid experiments were performed to identify which domains of Grb10ζ are responsible for oligomerization. These data indicated that the N-terminal region interacts with both the PH domain and the BPS-SH2 tandem domains and that BPS-SH2 does not self-associate. The latter result would seem to conflict with our crystallographic and solution findings. One possible explanation for some of these discrepancies is that Grb10ζ has a 58-residue extension on its N terminus *versus* Grb10γ, which could alter its self-association properties, although the BPS and SH2 domains are identical in all Grb10 isoforms.

The crystal structure of the Grb10 SH2 domain indicates that the binding pocket for the P+3 residue of a phosphopep-

tide ligand is absent because of a valine (Val-522) in the BG loop (BG3) rather than a glycine (Fig. 4, *A* and *B*), which is found at this position in the SH2 domains of, for example, Src and Abl (Fig. 3). In contrast to the N-terminal SH2 domain of p85 in which rotation of the Tyr-416 (BG5) side chain accommodates binding of the P+3 residue (43), a simple rotation of the (branched) Val-522 side chain in the Grb10 SH2 domain will not unmask a P+3 binding pocket. In addition to Val-522, the side chain of Asp-500 in the EF loop (EF1) extends into the space between the EF and BG loops in which the P+3 residue would normally bind (Fig. 4*B*). The side chain rotamer of Asp-500, a conserved residue in the Grb7/Grb10/Grb14 family, is stabilized through hydrogen bonding to several residues including Thr-504 (βF1) in the dimer interface.

Dimerization of the Grb10 SH2 domain is likely to fortify the positions of the EF and BG loops and thus contribute to ligand specificity. Although the residues in the interface of the Grb10 SH2 dimer are conserved in Grb7/Grb14, other residue differences in the SH2 domains of these proteins could affect the strength of the dimer interface. For example, a tyrosine in Grb10/Grb14 at position βB9 (Tyr-516 in Grb10), adjacent to Phe-515 in the center of the dimer interface (Fig. 1), is a histidine in Grb7, which might result in a weakened dimerization interface for the Grb7 SH2 domain.

Precedence for the lack of a P+3 binding pocket comes from the SH2 domain of Grb2, which shows strong specificity for phosphopeptides containing an asparagine at the P+2 position but no preference at the P+3 position (44). The crystal structure of the Grb2 SH2 domain shows that the bulky Trp-121 in the EF loop (EF1) forces the phosphopeptide to turn away from the SH2 domain at the P+2 position, facilitated by hydrogen bonds involving Asn(P+2) (39). Numerous studies have indicated that the SH2 domain of Grb7, like that of Grb2, has a preference for phosphopeptides with the turn-facilitating asparagine at the P+2 position (14, 15, 19, 20, 45), *e.g.* pTyr-1139 (pYV*N*Q) in Her2 (14). Thus, the hydrophobic residue in the BG loop, valine (Val-522) in Grb10/14 or isoleucine in Grb7, appears to function similarly to Trp-121 in the EF loop of Grb2, *i.e.* to discriminate against extended phosphotyrosine sequences and select for sequences that are predisposed to turn away from the surface of the SH2 domain after the phosphotyrosine.

In addition to influencing ligand specificity (through EF and BG loop stabilization), dimerization of the Grb10 SH2 domain would favor the binding of dimeric ligands such as the two β subunits of the insulin and IGF1 receptors. Interestingly, in the structures of the phosphorylated tyrosine kinase domains of these receptors (32, 46), the activation loop makes an abrupt turn after the first phosphotyrosine pTyr-1158/pTyr-1131 (insulin/IGF1 receptor). This conformation of the phosphorylated activation loop, including the turn after pTyr-1158/pTyr-1131, is stabilized by numerous interactions.

Differences in the phosphopeptide-binding properties of the Grb7/Grb10/Grb14 SH2 domains have been reported previously (5, 6, 24). With respect to binding to the phosphorylated insulin receptor, the SH2 domain of Grb7 appears to bind with the highest affinity followed by Grb10 and then Grb14 (6). In addition, the Grb7 SH2 domain interacts relatively strongly with pTyr-1139 (pYVNQ) in Her2 compared with the Grb14 SH2 domain (14). In the study by Janes *et al.* (14), selected Grb14 residues were swapped for the corresponding Grb7 residues and binding of the mutant Grb14 SH2 domains to pTyr-1139 in Her2 was measured. One of the key residues pinpointed was βD6, which is a leucine in Grb7 and a glutamine in Grb10/Grb14. Based on the Grb10 SH2 domain structure (with superimposed SH2-phosphopeptide structures), a leucine at βD6 can make favorable hydrophobic contacts with the phenolic ring of the phosphotyrosine. It should be noted that the βD6 residue is variable in SH2 domains and is often not a hydrophobic residue.

A non-glycl residue at the end of the five-residue BC loop of Grb7/Grb10/Grb14 family members, rare in SH2 domains, alters the conformation of the BC loop (Fig. 4*C*). Consequently, the residue difference between Grb7 and Grb10/Grb14 at BC2 (Ser-466 in Grb10) is probably also important in the tighter association of Grb7 with phosphopeptides. An arginine at this position in Grb7 is likely to interact with the phosphate group of the phosphotyrosine, whereas the shorter serine in Grb10/Grb14 might not directly coordinate the phosphate group. In SH2 domains with a glycine at BC5, the corresponding serine does hydrogen bond with the phosphate group (Fig. 4*C*). In addition, one or two hydrogen bonds typically made between the phosphate group and backbone nitrogen atoms in the tip of the BC loop could be compromised because of the non-glycl residue at BC5 in Grb7/Grb10/Grb14.

Based on the structural results presented here and biochemical results reported previously (4–6), we propose that the SH2 domains of Grb10/Grb14 are partially impaired in their ability to bind phosphotyrosine-containing ligands because of the non-glycl residue at the end of the BC loop and the lack of a P+3 binding pocket. Amino acid substitutions in the Grb7 SH2 domain such as leucine at βD6 (14), arginine at BC2 (predicted), and possibly others "rescue" the ability of Grb7 to bind phosphopeptides with reasonable affinity.

One plausible explanation for the reduced ligand binding capabilities of the Grb10/Grb14 SH2 domains is that the BPS domain, which is unique to this adapter family, also contributes to the interaction with the insulin and IGF1 receptors (4–6). Too high an overall affinity would alter the balance between Grb10/Grb14 binding and the binding of other downstream proteins. Indeed, isothermal titration calorimetry data (not shown) indicate that the tandem BPS-SH2 domains of Grb10 tightly associate with the phosphorylated insulin receptor kinase domain (IRK) (K_d <100 nM).

The relative contributions of the BPS and SH2 domains of Grb7/Grb10/Grb14 to insulin receptor binding varies. For Grb7, the interaction is mediated primarily by the SH2 domain (6), whereas for Grb14, the BPS domain predominates (5). In contrast, the two domains in Grb10 contribute approximately equally (4). Thus, engagement of Grb10 with the activated insulin receptor would appear to involve two modest affinity interactions that, in combination, provide high affinity and specificity.

The binding sites on the insulin receptor for the SH2 and BPS domains of Grb10 have not been unambiguously identified. In the context of full-length Grb10 (*i.e.* with the BPS domain present), the SH2 domain interacts with the phosphorylated activation loop of the insulin receptor (4, 11). The BPS domain also interacts with the core kinase domain, and, like the SH2 domain, binding requires phosphorylation of the activation loop (4). Yet from peptide competition experiments, the BPS domain does not appear to bind directly to the activation loop (23). The BPS domains of Grb10/14 have been shown to inhibit the catalytic activity of the insulin and IGF1 receptors (23, 24) in a manner that is non-competitive with ATP and non-competitive with substrate peptide (24). These data suggest that the BPS domain binds to a site on IRK distal to the active site, which becomes accessible only upon activation loop phosphorylation.

Based on the aforementioned studies and our gel-shift results that indicate formation of a 2:2 complex between Grb10 BPS-SH2 and phosphorylated IRK (Fig. 6*A*), we propose the

following interaction model for Grb10γ and the insulin receptor, as depicted in Fig. 6*B*. The SH2 dimer binds to the phosphorylated kinase activation loops in the two insulin receptor β subunits, with pTyr-1158 in the canonical phosphotyrosine-binding pocket of each SH2 domain. Yeast two-hybrid experiments demonstrate that pTyr-1162 and/or pTyr-1163 are critical for the interaction between the Grb10 SH2 domain and the insulin receptor, with pTyr-1158 less important (4, 11). The dependence on pTyr-1162/1163 is probably due in part to the role of these phosphotyrosines, especially pTyr-1163, in stabilization of the activation loop conformation (32). The aberrant BC loop (involved in phosphate coordination) in the Grb10 SH2 domain could explain why the substitution Tyr-1158 → Phe leads to only a modest decrease in binding of the SH2 domain, assuming additional interactions exist between the SH2 domain and IRK. The PH domain of Grb10γ is predicted to facilitate localization of Grb10γ to the plasma membrane, which will promote SH2 domain dimerization.

Acknowledgments—We thank J. Till and S. Li for assistance in synchrotron data collection and helpful discussions and N. Covino for technical support.

REFERENCES

1. Daly, R. J. (1998) *Cell. Signalling* **10,** 613–618
2. Kuriyan, J., and Cowburn, D. (1997) *Annu. Rev. Biophys. Biomol. Struct.* **26,** 259–288
3. Pawson, T., Gish, G. D., and Nash, P. (2001) *Trends Cell Biol.* **11,** 504–511
4. He, W., Rose, D. W., Olefsky, J. M., and Gustafson, T. A. (1998) *J. Biol. Chem.* **273,** 6860–6867
5. Kasus-Jacobi, A., Perdereau, D., Auzan, C., Clauser, E., Van Obberghen, E., Mauvais-Jarvis, F., Girard, J., and Burnol, A. F. (1998) *J. Biol. Chem.* **273,** 26026–26035
6. Kasus-Jacobi, A., Bereziat, V., Perdereau, D., Girard, J., and Burnol, A. F. (2000) *Oncogene* **19,** 2052–2059
7. Liu, F., and Roth, R. A. (1995) *Proc. Natl. Acad. Sci. U. S. A.* **92,** 10287–10291
8. O'Neill, T. J., Rose, D. W., Pillay, T. S., Hotta, K., Olefsky, J. M., and Gustafson, T. A. (1996) *J. Biol. Chem.* **271,** 22506–22513
9. Hansen, H., Svensson, U., Zhu, J., Laviola, L., Giorgino, F., Wolf, G., Smith, R. J., and Riedel, H. (1996) *J. Biol. Chem.* **271,** 8882–8886
10. Frantz, J. D., Giorgetti-Peraldi, S., Ottinger, E. A., and Shoelson, S. E. (1997) *J. Biol. Chem.* **272,** 2659–2667
11. Dong, L. Q., Farris, S., Christal, J., and Liu, F. (1997) *Mol. Endocrinol.* **11,** 1757–1765
12. Ooi, J., Yajnik, V., Immanuel, D., Gordon, M., Moskow, J. J., Buchberg, A. M., and Margolis, B. (1995) *Oncogene* **10,** 1621–1630
13. Stein, D., Wu, J., Fuqua, S. A., Roonprapunt, C., Yajnik, V., D'Eustachio, P., Moskow, J. J., Buchberg, A. M., Osborne, C. K., and Margolis, B. (1994) *EMBO J.* **13,** 1331–1340
14. Janes, P. W., Lackmann, M., Church, W. B., Sanderson, G. M., Sutherland, R. L., and Daly, R. J. (1997) *J. Biol. Chem.* **272,** 8490–8497
15. Yokote, K., Margolis, B., Heldin, C. H., and Claesson-Welsh, L. (1996) *J. Biol. Chem.* **271,** 30942–30949
16. Wang, J., Dai, H., Yousaf, N., Moussaif, M., Deng, Y., Boufelliga, A., Swamy, O. R., Leone, M. E., and Riedel, H. (1999) *Mol. Cell. Biol.* **19,** 6217–6228
17. Pandey, A., Duan, H., Di Fiore, P. P., and Dixit, V. M. (1995) *J. Biol. Chem.* **270,** 21461–21463
18. Stein, E., Cerretti, D. P., and Daniel, T. O. (1996) *J. Biol. Chem.* **271,** 23588–23593
19. Thommes, K., Lennartsson, J., Carlberg, M., and Ronnstrand, L. (1999) *Biochem. J.* **341,** 211–216
20. Jones, N., Master, Z., Jones, J., Bouchard, D., Gunji, Y., Sasaki, H., Daly, R., Alitalo, K., and Dumont, D. J. (1999) *J. Biol. Chem.* **274,** 30896–30905
21. Reilly, J. F., Mickey, G., and Maher, P. A. (2000) *J. Biol. Chem.* **275,** 7771–7778
22. Morrione, A., Valentinis, B., Resnicoff, M., Xu, S., and Baserga, R. (1997) *J. Biol. Chem.* **272,** 26382–26387
23. Stein, E. G., Gustafson, T. A., and Hubbard, S. R. (2001) *FEBS Lett.* **493,** 106–111
24. Bereziat, V., Kasus-Jacobi, A., Perdereau, D., Cariou, B., Girard, J., and Burnol, A. F. (2002) *J. Biol. Chem.* **277,** 4845–4852
25. Pace, C. N., Vajdos, F., Fee, L., Grimsley, G., and Gray, T. (1995) *Protein Sci.* **4,** 2411–2423
26. Minor, W., and Otwinowski, Z. (1997) *Methods Enzymol.* **276,** 307–326
27. Navaza, J. (1994) *Acta Crystallogr. Sec. A* **50,** 157–163
28. Peitsch, M. C. (1996) *Biochem. Soc. Trans.* **24,** 274–279
29. Futterer, K., Wong, J., Grucza, R. A., Chan, A. C., and Waksman, G. (1998) *J. Mol. Biol.* **281,** 523–537
30. Brunger, A. T., Adams, P. D., Clore, G. M., DeLano, W. L., Gros, P., Grosse-Kunstleve, R. W., Jiang, J. S., Kuszewski, J., Nilges, M., Pannu, N. S., Read, R. J., Rice, L. M., Simonson, T., and Warren, G. L. (1998) *Acta Crystallogr. Sec. D* **54,** 905–921
31. Jones, T. A., Zou, J. Y., Cowan, S. W., and Kjeldgaard, M. (1991) *Acta Crystallogr. Sec. A* **47,** 110–119
32. Hubbard, S. R. (1997) *EMBO J.* **16,** 5572–5581
33. Perkins, S. (1986) *Eur. J. Biochem.* **15,** 169–180
34. Jenkins, T., Engelman, A., Ghirlando, R., and Craigie, R. (1996) *J. Biol. Chem.* **271,** 7712–7718
35. Eck, M. J., Shoelson, S. E., and Harrison, S. C. (1993) *Nature* **362,** 87–91
36. Waksman, G., Shoelson, S. E., Pant, N., Cowburn, D., and Kuriyan, J. (1993) *Cell* **72,** 779–790
37. Rety, S., Futterer, K., Grucza, R. A., Munoz, C. M., Frazier, W. A., and Waksman, G. (1996) *Protein Sci.* **5,** 405–413
38. Schiering, N., Casale, E., Caccia, P., Giordano, P., and Battistini, C. (2000) *Biochemistry* **39,** 13376–13382
39. Rahuel, J., Gay, B., Erdmann, D., Strauss, A., Garcia-Echeverria, C., Furet, P., Caravatti, G., Fretz, H., Schoepfer, J., and Grutter, M. G. (1996) *Nat. Struct. Biol.* **3,** 586–589
40. Newcomer, M. E. (2002) *Curr. Opin. Struct. Biol.* **12,** 48–53
41. Shen, T. L., Han, D. C., and Guan, J. L. (2002) *J. Biol. Chem.* **277,** 29069–29077
42. Dong, L. Q., Porter, S., Hu, D., and Liu, F. (1998) *J. Biol. Chem.* **273,** 17720–17725
43. Nolte, R. T., Eck, M. J., Schlessinger, J., Shoelson, S. E., and Harrison, S. C. (1996) *Nat. Struct. Biol.* **3,** 364–374
44. Songyang, Z., Shoelson, S. E., Chaudhuri, M., Gish, G., Pawson, T., Haser, W. G., King, F., Roberts, T., Ratnofsky, S., Lechleider, R. J., Neel, B. G., Birge, R. B., Fajardo, J. E., Chou, M. M., Hanafusa, H., Schauffhausen, B., and Cantley, L. C. (1993) *Cell* **72,** 767–778
45. Pero, S. C., Oligino, L., Daly, R. J., Soden, A. L., Liu, C., Roller, P. P., Li, P., and Krag, D. N. (2002) *J. Biol. Chem.* **277,** 11918–11926
46. Favelyukis, S., Till, J. H., Hubbard, S. R., and Miller, W. T. (2001) *Nat. Struct. Biol.* **8,** 1058–1063